

## X-RAY LUMINOSITY FUNCTION AND TOTAL LUMINOSITY OF LOW-MASS X-RAY BINARIES IN EARLY-TYPE GALAXIES

DONG-WOO KIM AND GIUSEPPINA FABBIANO

Harvard-Smithsonian Center for Astrophysics, 60 Garden Street, Cambridge, MA 02138

Received 2003 December 3; accepted 2004 April 22

### ABSTRACT

We have derived bias-corrected X-ray luminosity functions (XLFs) of sources detected in a uniformly selected sample of 14 E and S0 galaxies observed with *Chandra* ACIS-S3. The entire sample yields 985 pointlike X-ray sources, with typical detections of 30–140 sources per galaxy. After correcting for incompleteness, the individual XLFs are statistically consistent with a single power law of a (differential) XLF slope  $\beta = 1.8\text{--}2.2$  (with a typical error of 0.2–0.3). A break at or near  $L_{X, \text{Edd}}$ , as reported in the literature for some of these galaxies, is not required in any case. Given the uniform XLF shape, we have generated a combined, higher statistics XLF, representative of X-ray sources in elliptical galaxies. Although the combined XLF is marginally consistent with a single power law (with  $\beta = 2.1 \pm 0.1$ ), a broken power law gives an improved fit. The best-fit slope is  $\beta = 1.8 \pm 0.2$  in the low-luminosity range  $L_X = \text{a few} \times 10^{37}$  to  $5 \times 10^{38}$  ergs  $\text{s}^{-1}$ . At higher luminosities, the slope is steeper,  $\beta = 2.8 \pm 0.6$ . The break luminosity is  $(5 \pm 1.6) \times 10^{38}$  ergs  $\text{s}^{-1}$  (with an error at 90%), which may be consistent with the Eddington luminosity of neutron stars with the largest possible mass ( $3 M_\odot$ ), He-enriched neutron star binaries, or low-mass stellar-mass black holes. If the change in XLF slope at high luminosities is real and does not mask a step in the XLF, our result would imply a different population of high-luminosity sources, instead of a beaming effect. This high-luminosity portion of the XLF must reflect the mass function of black holes in these galaxies. We note that this high-luminosity population does not resemble that of the ultraluminous X-ray sources detected in star-forming galaxies, where no break in the XLF is present and the XLF is much flatter than in the older stellar system we are studying here. We use our results to derive the integrated X-ray luminosity of accreting low-mass X-ray binaries (LMXBs) in each sample galaxy. We confirm that the total X-ray luminosity of LMXBs is correlated with the optical and more tightly with the near-IR luminosities, but in both cases the scatter exceeds that expected from measurement errors. We find that the scatter in  $L_X(\text{LMXB})/L_K$  is marginally correlated with the specific frequency of globular clusters.

*Subject headings:* galaxies: elliptical and lenticular, cD — X-rays: binaries — X-rays: galaxies

*Online material:* color figures

### 1. INTRODUCTION

With its subarcsecond spatial resolution and unprecedented sensitivity (Weisskopf et al. 2000), *Chandra* has provided incontrovertible proof of the existence of populations of low-mass X-ray binaries (LMXBs) in all E and S0 galaxies (e.g., Sarazin et al. 2001; Angelini et al. 2001; Kim & Fabbiano 2003, hereafter KF03). Prior to *Chandra*, there was good but indirect evidence of the existence of these LMXBs (see Fabbiano 1989). This evidence included both statistical considerations and the spectral properties of the integrated X-ray emission. The former were based on the observation that the lower envelope of the X-ray/optical luminosity distribution of E and S0 galaxies is consistent with the integrated output of their stellar population and X-ray binary component, inferred from the extrapolation of the properties of the bulge of M31 (e.g., Trinchieri & Fabbiano 1985; Eskridge et al. 1995). The latter evidence was the detection of a hard spectral component, typical of LMXBs, in both the *Einstein* (Kim et al. 1992) and more strikingly in the wide-beam *ASCA* spectra (Matsushita et al. 1994) of these galaxies; this hard emission, however, could also have stemmed from low-luminosity or absorbed active galactic nuclei (AGNs; e.g., Allen et al. 2000). The *Chandra* images reveal populations of pointlike sources in all E and S0 galaxies. The *Chandra* ACIS spectra of these sources are hard, as would be

expected from LMXBs (see review in Fabbiano & White 2003).

The detection of X-ray source populations in galaxies with *Chandra* has created a veritable industry in the derivation of the X-ray luminosity functions (XLFs) of these populations (see Fabbiano & White 2003 and references therein). Comparison of XLFs of different star-forming galaxies provides empirical evidence of differences in their star formation history (e.g., Gilfanov et al. 2003). Comparison with X-ray binary evolution models tailored to the different stellar populations shows that predictions and consistency checks for both the shape and the normalization of XLFs are possible with theoretical X-ray binary modeling (Belczynski et al. 2004). These results show that the XLFs of sources in a given galaxy (or galactic region) reflect the formation, evolution, and physical properties of the X-ray source population.

The XLFs of the E and S0 galaxies observed with *Chandra* are generally steeper than those of star-forming galaxies and are fitted with power laws (or broken power laws) with reported cumulative slopes ranging from 1.0 to 1.8. Breaks have been reported both at luminosities of  $\sim 2 \times 10^{38}$  ergs  $\text{s}^{-1}$ , near the Eddington luminosity of neutron stars (e.g., Sarazin et al. 2000; Blanton et al. 2001; Kundu et al. 2002), and at higher luminosities near  $10^{39}$  ergs  $\text{s}^{-1}$  (Jeltema et al. 2003). While the former break may be related to a transition between neutron star and black hole binaries as the main contributors

to a given luminosity range (Sarazin et al. 2000), the high-luminosity break could be produced by an aging “younger” component from binaries formed in rejuvenation (merging) episodes (Jeltema et al. 2003).

These results (and conclusions), however, may be affected by incompleteness effects, as demonstrated by KF03 in the case of NGC 1316. Low-luminosity sources may be missed in the inner region of galaxies because of the increased background levels from the more intense diffuse emission (see also Zezas & Fabbiano 2002). At larger radii, the detection sensitivity is affected by the widening of the *Chandra* point-spread function. In NGC 1316, these effects resulted in an apparent break at  $\sim 2 \times 10^{38}$  ergs s<sup>-1</sup> that disappeared, producing a straight power law once the incompleteness corrections were applied. This result affects both our understanding of the X-ray population of NGC 1316 and also the estimate of the integrated contribution of fainter LMXBs to the total unresolved X-ray emission. As discussed in KF03, the latter would affect both the measure of the metal abundances of the hot interstellar medium (ISM) and measurements that rely on the knowledge of the properties of the hot ISM, such as the determination of the binding mass of the galaxy assuming hydrostatic equilibrium.

The purpose of the work reported in this paper is to explore how typical the results of KF03 are. We extended our study to a well-defined sample of 14 E and S0 galaxies, all observed with the ACIS-S3 CCD chip. All the data used in this work were retrieved from the public *Chandra* archive, and some of them have been used in publications by the original *Chandra* investigators. For all these galaxies we have derived bias-corrected XLFs, with incompleteness corrections (following KF03) applied in all cases.

This paper is organized as follows. In § 2 we describe our sample selection and data reduction technique. In § 3 we first derive and correct for incompleteness the XLF of each galaxy in the sample, concluding that all are consistent with each other within statistics; we then derive a combined XLF for the entire sample to increase our sensitivity. In § 4 we use these results to calculate the total X-ray luminosity of LMXBs and its ratio to the galaxy optical luminosity, using both detected and undetected LMXBs. In § 5 we discuss the features of the composite XLF, and we compare our derived LMXB integrated luminosities with both galactic optical (stellar) luminosities and the globular cluster (GC) specific frequency to set constraints on LMXB formation and evolution scenarios. Finally, we summarize our conclusions in § 6.

## 2. SAMPLE SELECTION AND DATA REDUCTION

To build XLFs for a sizeable sample of early-type galaxies, we have extracted data from the *Chandra* public archive<sup>1</sup> according to the following selection criteria: (1) we have selected only early-type galaxies with morphological type  $T < 0$  (taken from the Third Reference Catalogue of Bright Galaxies [de Vaucouleurs et al. 1991, hereafter RC3]), which (2) were the targets of *Chandra* pointings, resulting in the best possible angular resolution and point-source detection sensitivity; (3) to minimize instrumental effects, we have used only data taken with the ACIS-S3 (back-illuminated) CCD chip, which is better calibrated than the front-illuminated chips and is also more sensitive at low energies; (4) to ensure low enough detection thresholds, we have further restricted the sample to include only observations with exposure times longer than

20 ks, after background flare screening; finally, (5) we require that there be more than 30 detected point sources, detected within the  $D_{25}$  ellipse (25th magnitude isophote, taken from RC3) of a given galaxy, so as to have a reasonable determination of the XLF. Our selection method ensures that our sample consists of uniform data and that the instrumental effects can be corrected with best-known calibration data. The resulting sample consists of 14 early-type galaxies. Their basic properties are listed in Table 1, together with the published papers on these data. We take the distance from the surface brightness fluctuation results by Tonry et al. (2001). For galaxies in the Virgo and Fornax Clusters we adopt the group distance, and for the remaining galaxies we use individual measurements. For all galaxies except three, the data were acquired after the ACIS temperature reached  $-120^\circ\text{C}$  (which is the best-calibrated state so far). The gain correction is less accurate for NGC 1399, NGC 4636, and NGC 4697, and hence spectral information may suffer from larger systematic uncertainties for these galaxies. However, the broadband photometry needed for this study would not be significantly affected.

We have uniformly reduced the ACIS data with XPIPE (Kim et al. 2004a), a suite of software specifically developed for the *Chandra* Multiwavelength Project (ChaMP). XPIPE takes the CXC pipeline level 2 data products and then applies additional corrections (e.g., gain correction, removing bad pixels/columns) and screening (e.g., removing background flares). For details, we refer to Kim et al. (2004a). To detect X-ray sources, we used the CIAO<sup>2</sup> *wavdetect* tool (Freeman & Kashyap 2002). As discussed in KF03 and Kim et al. (2004a), the performance and limitations of *wavdetect* are well understood and calibrated by extensive simulations.

We determined source fluxes in the 0.3–8 keV band by applying an energy conversion factor (ECF) to the detected source count rate. The ECFs had to be tailored to each observation, because the quantum efficiency (QE) of ACIS varies with time (for the QE degradation, see the CXC memo of 2002 July 29<sup>3</sup>) and because the Galactic value of  $N_{\text{H}}$  varies from one pointing to another. To calculate the ECF, we assume a power-law emission model of  $\Gamma_{\text{ph}} = 1.7$  with absorption by Galactic  $N_{\text{H}}$  determined for each observation (Stark et al. 1992) and use the CIAO Sherpa package in conjunction with *corrarf*, a tool that corrects the instrumental response files to take into account the variation of the QE.<sup>4</sup> We find that the ECFs vary by  $\sim 25\%$  within our sample.

## 3. X-RAY LUMINOSITY FUNCTIONS

To construct the XLF of the X-ray source population of a given galaxy, we restricted the sample of detected pointlike sources according to the following criteria. (1) In the case of large galaxies (e.g., NGC 1316 and NGC 4472), where part of the emission falls outside the S3 chip (in the adjacent front-illuminated chips), we ignored these outer sources to avoid uncertainties introduced by the different instrumental responses. (2) We used only X-ray sources detected within the  $D_{25}$  ellipse of each galaxy. While some sources found outside the  $D_{25}$  ellipse could be associated with the galaxy under study, the contamination by background sources would be increased significantly by including these larger areas. Within the  $D_{25}$  ellipse, on average we expect only about 10% contamination

<sup>2</sup> See <http://cxc.harvard.edu/ciao>.

<sup>3</sup> Available at [http://cxc.harvard.edu/cal/Acis/Cal\\_prods/qeDeg/index.html](http://cxc.harvard.edu/cal/Acis/Cal_prods/qeDeg/index.html).

<sup>4</sup> Sherpa and *corrarf* are available at <http://cxc.harvard.edu/sherpa> and [http://cxc.harvard.edu/cal/Acis/Cal\\_prods/qeDeg/2003\\_11\\_19/corraf.tar.gz](http://cxc.harvard.edu/cal/Acis/Cal_prods/qeDeg/2003_11_19/corraf.tar.gz).

<sup>1</sup> See <http://asc.harvard.edu/cda>.

TABLE 1  
SAMPLE GALAXIES

NAME (1)	OBS. ID (2)	OBS. DATE (3)	$N_{\text{H}}$ (4)	ECF (5)	$D$ (6)	$T$ TYPE (7)	$D_{25}$ (8)	$B_T^0$ (9)	$K_{20}$ (10)	$S_{\text{GC}}$ (11)	EXPOSURE		NUMBER OF SOURCES				REFERENCE (18)
											Before (12)	After (13)	S3 (14)	$D_{25}$ (15)	$r > 20''$ (16)	Bkgd. (17)	
I1459.....	2196	2001 Aug 12	1.17	72.958	29.0	−5	5.25	10.83	6.929	...	60166	53055	74	59	44	5	1
N0720.....	492	2000 Oct 12	1.57	69.810	28.0	−5	4.68	11.13	7.393	1.0	40124	32802	69	36	30	2	2
N1316.....	2022	2001 Apr 17	2.13	72.202	19.9F	−2	12.02	9.40	5.688	2.5	30233	24683	83	77	66	10	3
N1399.....	319	2000 Jan 18	1.50	63.209	19.9F	−5	6.92	10.44	6.440	8.6	56659	55645	181	142	139	6	4
N1407.....	791	2000 Aug 16	5.43	77.391	29.0	−5	4.57	10.71	6.855	...	49196	42352	146	87	82	5	
N3379.....	1587	2001 Feb 13	2.78	74.407	11.0	−2	5.37	10.18	6.362	1.1	31923	28851	69	44	27	5	
N4365.....	2015	2001 Jun 2	1.61	73.200	17.0V	−5	6.92	10.49	6.800	6.3	40947	38748	135	112	101	7	5
N4374.....	803	2000 May 19	2.78	69.746	17.0V	−5	6.46	10.01	6.347	2.4	28841	27587	86	65	54	7	6
N4382.....	2016	2001 May 29	2.50	75.163	17.0V	−1	7.08	9.99	6.260	...	40259	37477	71	50	41	8	5
N4472.....	321	2000 Jun 12	1.62	67.578	17.0V	−5	10.23	9.33	5.506	3.9	40096	33568	136	129	123	10	7
N4621.....	2068	2001 Aug 1	2.17	75.073	17.0V	−5	5.37	10.53	6.866	5.5	25155	23354	72	42	30	3	
N4636.....	323	2000 Jan 26	1.82	64.208	17.0V	−5	6.03	10.43	6.628	6.5	53049	42408	101	65	61	4	8
N4649.....	785	2000 Apr 20	2.13	67.607	17.0V	−5	7.41	9.70	5.825	6.0	37350	21536	141	119	116	6	9
N4697.....	784	2000 Jan 15	2.14	64.699	12.0	−5	7.24	10.07	6.502	4.4	39763	36663	91	73	70	7	10

NOTES.—Col. (1): Galaxy name. Col. (2): *Chandra* observation ID. Col. (3): *Chandra* observation date. Col. (4): Galactic  $N_{\text{H}}$  in units of  $10^{20} \text{ cm}^{-2}$  (taken from Stark et al. 1992). Col. (5): Energy conversion factor in units of  $10^{-13} \text{ ergs s}^{-1} \text{ cm}^{-2}$  per 1 count  $\text{s}^{-1}$ . Col. (6): Distance in Mpc (Tonry et al. 2001). Note that for galaxies in the Fornax (F) and Virgo (V) Clusters, we use the group distance. Col. (7): Morphological type (taken from RC3). Col. (8): Diameter at the 25th magnitude isophote in arcminutes (taken from RC3). Col. (9): Total face-on  $B$  magnitude corrected for Galactic extinction (taken from RC3). Col. (10): 2MASS  $K$  magnitude within the 20 mag arcsec $^{-2}$  isophote (Jarrett et al. 2003). Col. (11): Specific frequency of GCs taken (and corrected for our distances) from Goudfrooij et al. (2001) for NGC 1316, Rhode & Zepf (2004) for NGC 3379 and NGC 4472, Gomez & Richtler (2004) for NGC 4374, and Kissler-Patig (1997) for the rest of the galaxies. There are no available data for NGC 1407, NGC 4382, and IC 1459. Col. (12): Effective exposure time in seconds before excluding background flares. Col. (13): Effective exposure time in seconds after excluding background flares. Col. (14): Number of sources in the S3 chip. Col. (15): Number of sources within the  $D_{25}$  ellipse in the S3 chip. Col. (16): Number of sources at  $r > 20''$  within the  $D_{25}$  ellipse in the S3 chip. Col. (17): Number of expected background sources in the same region as in col. (16) (based on  $\log N - \log S$  in Kim et al. 2004b). Col. (18): References to previous works on the individual *Chandra* observations.

REFERENCES.—(1) Fabbiano et al. 2003; (2) Jeltema et al. 2003; (3) KF03; (4) Angelini et al. 2001; (5) Sivakoff et al. 2003; (6) Finoguenov & Jones 2002; (7) Kundu et al. 2002; (8) Jones et al. 2002 (no discussion about LMXBs); (9) Randall et al. 2004; (10) Sarazin et al. 2000.

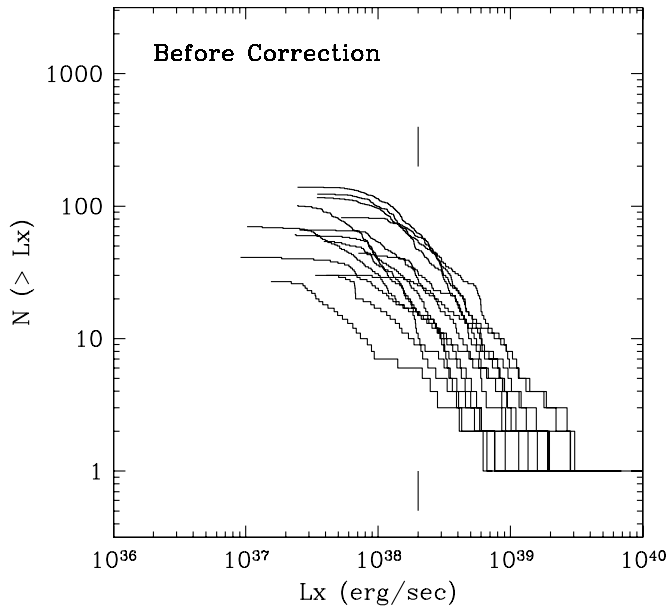


FIG. 1a

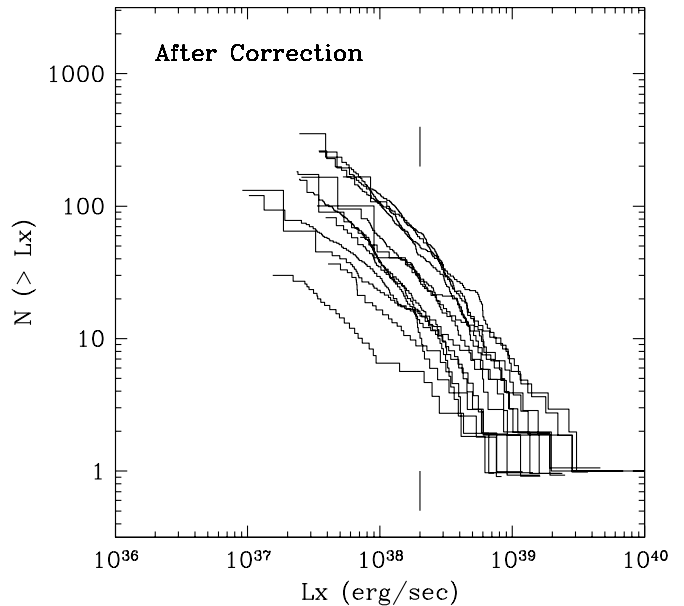


FIG. 1b

FIG. 1.—(a) Uncorrected XLFs of LMXBs for 14 early-type galaxies listed in Table 1. (b) Bias-corrected XLFs of LMXBs. The location of the Eddington luminosity ( $2 \times 10^{38}$  ergs  $s^{-1}$ ) of a  $1.4 M_{\odot}$  neutron star is marked by vertical bars. [See the electronic edition of the *Journal* for a color version of this figure.]

by background sources, on the basis of the  $\log N - \log S$  relation of the ChaMP survey (Kim et al. 2004b). (3) We excluded sources found within  $20''$  of the galaxy center to avoid contamination by nuclear sources, to minimize confusion effects in the crowded central regions, and to reduce the biases on the detection thresholds resulting from the more intense hot ISM emission of these inner regions. We note that this will not affect our results because there is no systematic difference between radial distributions of X-ray-bright and X-ray-faint sources (E. Kim et al. 2004, in preparation).

With the above restrictions, we derive a total number of 985 sources from our sample of 14 galaxies, ranging from 30 to 140 sources per galaxy. The individual—uncorrected—cumulative XLFs are shown in Figure 1a. The location of  $L_{X,\text{Edd}} = 2 \times 10^{38}$  ergs  $s^{-1}$  is marked by vertical bars near the top and bottom of the figure. The XLFs appear to be following simple power laws at the high- $L_X$  end and to flatten at the low- $L_X$  side. As we show below, this flattening is mostly the result of incompleteness effects.

### 3.1. Incompleteness Correction

As shown by KF03, the apparent flattening of the XLFs at the low luminosities may stem from incompleteness effects. A full list of these effects includes the following: (1) the effect of the strong diffuse emission present in E and S0 galaxies (from hot ISM) on the detection probability for faint sources, (2) the Eddington bias, which causes a spurious apparent increase of sources detected near the threshold, (3) confusion effects, and (4) the effect of the increasing point-spread function at larger radii on the source detection thresholds.

To assess the correction to be applied to each *observed* XLF, we have followed the “backward” method outlined in Appendix B of KF03, which corrects all the above effects at the same time. This method consists of running a series of simulations for each galaxy, adding one source at a time to the real observational data within the defined spatial region ( $r > 20''$  and within the  $D_{25}$  ellipse), and determining whether the inserted source could be detected by the same technique used for

the *Chandra* data. We ran 20,000 simulations per galaxy. The “added” source was selected with a random  $L_X$  based on a single power law XLF with  $\alpha = 1$  in a cumulative form,

$$N(>L_X) \sim L_X^{-\alpha},$$

and placed in a random location based on the optical light distribution assuming the  $r^{1/4}$  law (de Vaucouleurs 1948; see also § 5.3). Note that the input XLF used for these simulations is not critical because we are only using the ratio of the number of input to output (i.e., detected) sources to estimate the correction to the XLFs at each luminosity. The corrected XLFs are shown in Figure 1b. The XLF shapes are all remarkably similar apart from the factor  $\sim 20$  spread in normalization at  $L_X \sim 10^{38}$  ergs  $s^{-1}$ . The apparent strong XLF breaks near  $L_{X,\text{Edd}}$  visible in Figure 1a mostly disappear after the corrections are applied.

### 3.2. The Shapes of Individual XLFs

Figure 2 (same as Fig. 1b but rescaled by arbitrary factors for visibility) shows a variety of XLF shapes in our 14 galaxy sample. Is this variety due to intrinsic differences in the XLFs, or is it driven by small-number statistics? Remember that 30–140 sources are detected in each galaxy. To address this question, we again resorted to simulations, generating 100 simulated XLFs selected from the same parent population. From the 20,000 simulations generated for NGC 1399 with a single power law with a slope  $\alpha = 1$  (see § 3.1), we selected 100 sets of 100 detected sources randomly. The XLFs derived from these simulations are then corrected by the ratio of input and detected number of sources, as discussed in § 3.1. The corrected XLFs are plotted in Figure 3 (we plot only 10 XLFs for visibility), which can be directly compared with Figures 1b and 2. As expected, the apparent XLF flattening at lower luminosities disappears in the corrected XLFs. In spite of the fact that they were all drawn from the same parent population, the simulated XLFs of Figure 3 have different shapes. This apparent variety appears consistent with that observed in the

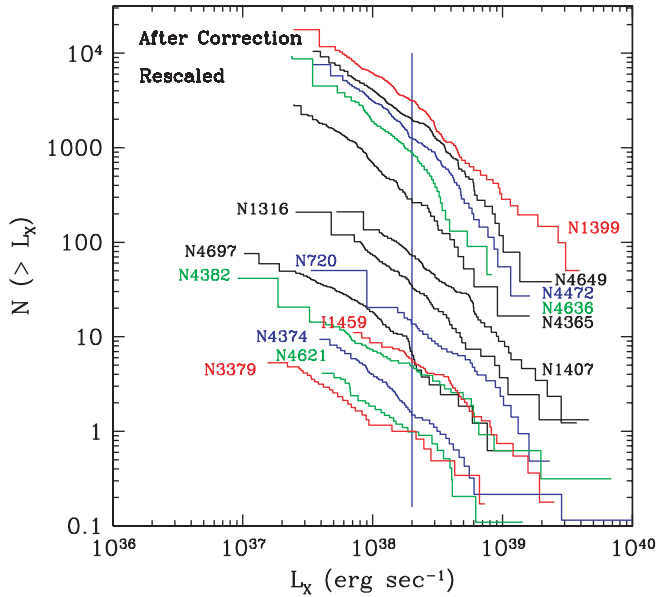


FIG. 2.—Same as Fig. 1*b*, but rescaled by arbitrary factors (numbers in parentheses below) for visibility. From top to bottom are NGC 1399 (*red*; 50.12), NGC 4649 (*black*; 39.81), NGC 4472 (*blue*; 29.51), NGC 4636 (*green*; 50.12), NGC 4365 (*black*; 17.78), NGC 1407 (*black*; 1.26), NGC 1316 (*black*; 1.26), NGC 720 (*blue*; 0.50), NGC 4697 (*black*; 0.63), IC 1459 (*red*; 0.19), NGC 4382 (*green*; 0.32), NGC 4374 (*blue*; 0.12), NGC 4621 (*green*; 0.11), and NGC 3379 (*red*; 0.18). The location of the Eddington luminosity ( $2 \times 10^{38}$  ergs  $s^{-1}$ ) of a  $1.4 M_{\odot}$  neutron star is marked by a vertical line.

real XLFs and simply reflects the limitation of small-number statistics.

We have fitted the XLFs with a variety of methods to derive best-fit parameters, goodness of fit, and confidence intervals. These methods include the maximum likelihood method (ML; Crawford et al. 1970), the Kolmogorov-Smirnov (K-S) test, the minimum  $\chi^2$  method, the *c*-statistic (cstat), and the Cash statistic (the last three are available in the CIAO Sherpa package). Cash and cstat are similar to the ML method. Of these methods, the minimum  $\chi^2$  method is the best calibrated (and hence most extensively used, for example in X-ray spectral fitting) and can provide best-fit parameters, confidence intervals, and an estimate of goodness of fit. However, it requires binned data. The other methods work with unbinned data but only provide limited statistical information (e.g., only best-fit parameters for ML and only goodness of fit for K-S).

Since the errors in the cumulative XLF are not independent, we apply the statistical tests to the differential XLF given by

$$\frac{dN}{dL_X} = KL_X^{-\beta}.$$

For a single power law,  $\beta = \alpha + 1$ , where  $\alpha$  is the power-law index of the cumulative XLF (defined in § 3.1), while for a broken power law,  $\beta = \alpha + 1$  holds only above the break luminosity;  $\beta < \alpha + 1$  below the break. We also note that the confidence ranges determined by the cstat and Cash statistics are not reliable because the corrected XLFs do not follow Poisson statistics.

The results of the fit are summarized in Table 2. The errors quoted in the table (and throughout this paper) are at the 90% confidence level, unless specified otherwise. The results of cstat and Cash are similar to those of ML and are not listed.

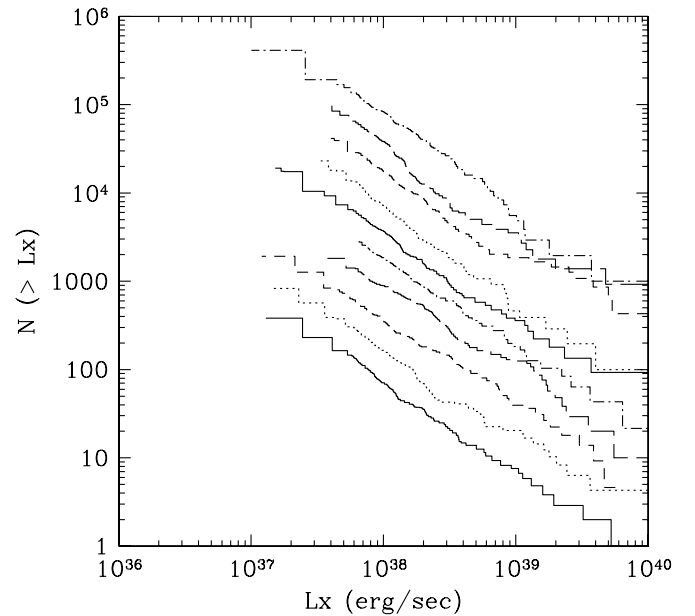


FIG. 3.—Ten simulated XLFs with 100 sources drawn from the same parent population of an XLF (differential) slope of 2 after correction. They are directly compared with Figs. 1*b* and 2. They are arbitrarily rescaled for visibility. [See the electronic edition of the *Journal* for a color version of this figure.]

With the K-S test, we estimated the best-fit parameter via a grid-search method, as described in Fasano et al. (1993). Because the statistic *D* in the K-S test is not fully calibrated and the best-fit parameter determined by the K-S method may not be reliable, we only use the K-S results in conjunction with other test results. For the minimum  $\chi^2$  fits, we binned the data to have at least 10 (uncorrected) sources in each bin.

The bias-corrected XLF of individual galaxies is well reproduced by a single, unbroken power law. The differential best-fit slopes are  $\beta = 2.0 \pm 0.2$  for most galaxies. In a few galaxies with smaller numbers of sources ( $< 50$ ), the slope is slightly flatter,  $\beta = 1.7 \pm 0.4$ , but still consistent with those of the main group. We note that none of the XLF fits can formally exclude a single power law (the probability in cols. [4] and [8] of Table 2 is always larger than 20%). NGC 4697 is the only galaxy with an XLF, which may suggest (but not require) a more complex model than a single power law. However, the statistics are still marginal (6% and 46% in the K-S and minimum  $\chi^2$  tests, respectively).

For comparison, we have fitted the simulated XLFs in the same way as the real XLFs in Table 2. This test also allows us to estimate the size of systematic errors in our approach. Note that the simulated XLFs were all made with 100 sources (before bias correction) taken from the same parent population. The best-fit slope of the 100 simulated XLFs ranges from  $\beta = 1.8$  to 2.2, with a typical error of  $\sim 0.2$ , or  $\sim 8\%$  (at 90% confidence). Similarly, the best-fit amplitude varies by  $\sim 12\%$  (at 90% confidence). In Figure 4 we compare the best-fit slopes determined by the minimum  $\chi^2$  method (col. [5] in Table 2) for the simulated XLFs (Fig. 3) and real bias-corrected XLFs (Fig. 1*b*). The spread of the best-fit slope of simulated XLFs is similar to that of the real bias-corrected XLFs, indicating that the spread in the real XLFs is within the range of expected error. Our result demonstrates that the apparent variety of XLF shapes could be an artifact of poor count statistics. Moreover, models more complex than single power laws are not required by the data.

TABLE 2  
FITTING OBSERVED X-RAY LUMINOSITY FUNCTIONS

NAME (1)	ML $\beta$ (2)	K-S		$\chi^2$ METHOD				
		$\beta$ (3)	Probability (%) (4)	$\beta$ (5)	Amplitude (6)	$\chi^2_{\text{reduced}}$ (7)	$\chi^2/\text{dof}$ (8)	Probability (%) (9)
I1459.....	1.66	1.80	39.24	$1.70^{+0.31}_{-0.30}$	$39.14^{+19.07}_{-16.26}$	0.39	1.16/3	76.21
N0720.....	1.96	1.97	100.00	$1.62^{+0.67}_{-0.83}$	$33.01^{+57.79}_{-27.05}$	0.42	0.42/1	51.71
N1316.....	2.16	1.97	96.52	$2.13^{+0.26}_{-0.23}$	$61.93^{+17.52}_{-17.03}$	0.25	1.23/5	94.23
N1399.....	2.02	1.95	84.66	$2.00^{+0.17}_{-0.16}$	$111.14^{+22.48}_{-21.98}$	0.97	11.64/12	47.48
N1407.....	2.07	1.98	97.47	$2.11^{+0.29}_{-0.28}$	$132.01^{+61.87}_{-49.96}$	0.79	5.54/7	59.41
N3379.....	1.62	1.80	44.84	$1.73^{+0.40}_{-0.35}$	$6.73^{+2.34}_{-2.49}$	1.07	1.07/1	30.11
N4365.....	1.94	1.94	82.95	$1.94^{+0.20}_{-0.18}$	$38.57^{+6.72}_{-6.73}$	0.97	7.79/8	45.41
N4374.....	1.88	2.00	97.97	$2.18^{+0.25}_{-0.22}$	$39.09^{+10.28}_{-10.34}$	0.55	2.19/4	70.06
N4382.....	1.69	1.90	99.65	$1.72^{+0.37}_{-0.33}$	$17.48^{+6.39}_{-6.66}$	0.15	0.29/2	86.36
N4472.....	2.03	2.02	70.98	$2.10^{+0.22}_{-0.20}$	$117.08^{+25.54}_{-25.06}$	0.75	8.23/11	69.23
N4621.....	1.86	1.96	86.16	$1.79^{+0.72}_{-0.54}$	$15.30^{+5.57}_{-5.99}$	1.63	1.63/1	20.11
N4636.....	2.10	2.04	93.78	$2.10^{+0.33}_{-0.35}$	$46.93^{+13.66}_{-14.13}$	0.79	3.14/4	53.44
N4649.....	1.98	2.01	98.60	$1.97^{+0.22}_{-0.20}$	$113.52^{+30.30}_{-28.32}$	0.98	9.80/10	45.79
N4697.....	1.53	1.80	6.05	$1.67^{+0.20}_{-0.19}$	$21.55^{+4.55}_{-4.55}$	0.92	4.61/5	46.54

NOTES.—Col. (1): Galaxy name. Col. (2): Best-fit  $\beta$  determined by the maximum likelihood method. Cols. (3)–(4): Best-fit  $\beta$  determined by the K-S grid search and the corresponding probability. Col. (5): Best-fit  $\beta$  and its error at the 90% confidence level determined by the  $\chi^2$  method. Col. (6): Best-fit amplitude and its error at the 90% confidence level determined by the  $\chi^2$  method. Cols. (7)–(8): Reduced  $\chi^2$  and  $\chi^2/\text{degrees of freedom}$  determined by the  $\chi^2$  method. Col. (9): Probability determined by the  $\chi^2$  method.

However, we find a significant effect when we compare the amplitudes of the XLFs, which is not surprising since the same galaxy was used for generating the simulated XLF, while the real XLF reflects a range of galactic population sizes. The amplitude of the XLF (col. [6]), which is a measure of the total number of X-ray sources, varies considerably by a factor of  $\sim 20$  from one galaxy to another (or by a factor of  $\sim 3$  after normalizing by  $L_K$ ; see § 4). For comparison, the amplitude in the simulation test varies only within  $\sim 12\%$ . We discuss the

implications of this result for the scatter of  $L_X(\text{LMXB})$  and its ratio to the optical luminosity in § 4.

### 3.3. Combined XLF

As shown in § 3.2, all the bias-corrected XLF slopes are consistent within the errors. We therefore combined them to increase the statistical significance of our data. Because the range of  $L_X$  covered by the XLF is different from one galaxy to another, we used the combined XLF only in the luminosity

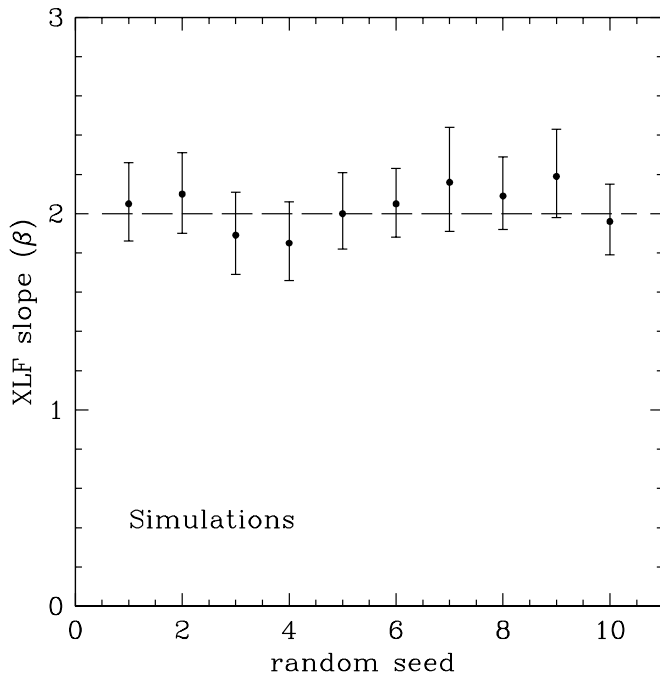


FIG. 4a

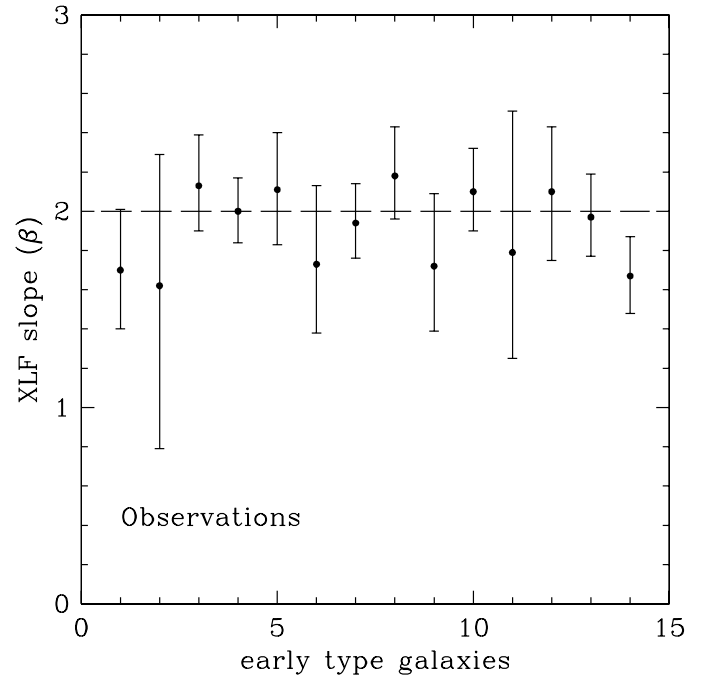


FIG. 4b

FIG. 4.—Distribution of the best-fit XLF slopes for (a) simulations and (b) observations. The simulated XLFs are made with 100 LMXBs, while those observed are made with 30–140 LMXBs.

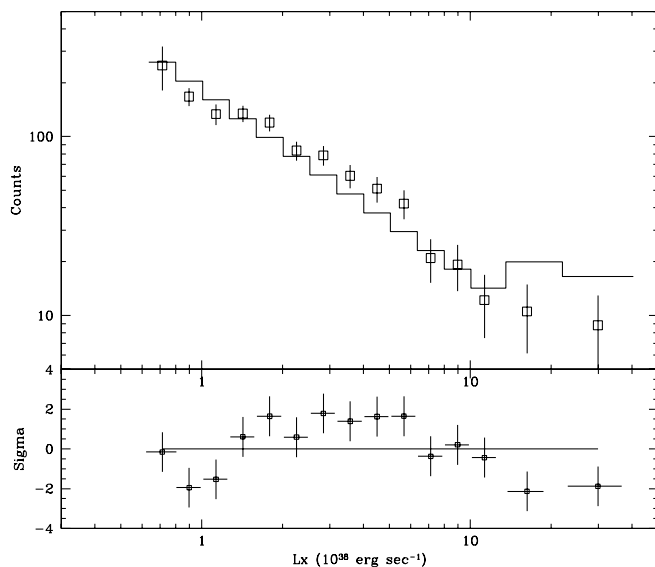


FIG. 5a

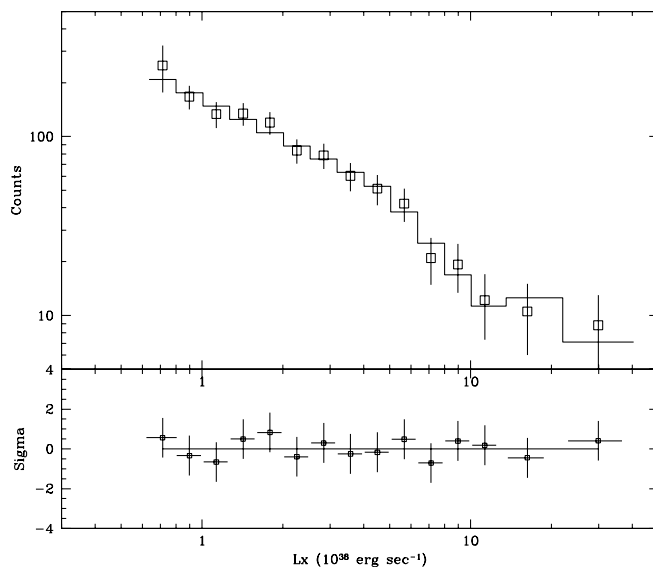


FIG. 5b

FIG. 5.—Fit of the combined (differential) XLF to (a) a single power law and (b) a broken power law.

range  $L_X > 6 \times 10^{37}$  ergs  $s^{-1}$ , for which all the galaxies give detections. This combined XLF includes 874 sources and is plotted in Figure 5. In fitting the combined XLF, we take into account various errors. First, we determine the statistical error by Poisson statistics. Second, we add the systematic error estimated in § 3.2, which is 12% at 90%, or 7% at 1  $\sigma$ . Third, we also add the distance error. While group distance errors for the Virgo and Fornax galaxies are small ( $\sim 2\%$ ), individual distance errors for our 14 galaxies are  $\sim 8\%$  (Tonry et al. 2001). We have compared the two cases using group distances and individual galaxy distances, but the results are consistent with each other. The only noticeable difference (although still consistent within the errors) is that the break luminosity, when a broken power law model is used, is slightly higher (by  $\sim 10\%$ ) in the latter case, with a slightly larger error. To properly consider these errors in determining the XLF parameters and their errors, we have used a Monte Carlo technique by applying the statistical and systematic errors to the number of sources (i.e., vertical variation of XLF) and the distance error to  $L_X$  (i.e., horizontal variation of XLF). Note that applying the systematic and distance errors in addition to the statistical error does not significantly change the best-fit parameters, but makes their acceptable ranges (or errors) larger.

A fit with a single power law of this XLF (Fig. 5b) yielded the best-fit single power law slope,  $\beta = 2.1 \pm 0.1$ , consistent with the individual XLF fits but with a smaller error. Formally, a single power law is marginally acceptable with typical  $\chi^2_{\text{reduced}} = 2.0$  for 13 degrees of freedom ( $\sim 1\%$  probability of exceeding the  $\chi^2$  statistic).

Fitting the XLF with a broken power law model results in a better fit, with  $\chi^2_{\text{reduced}}$  close to 1 for 11 degrees of freedom (Fig. 5b). The  $F$ -test indicates that the probability of exceeding  $F$  is  $\sim 1\%$ . The best-fit break luminosity is  $(5.0 \pm 1.6) \times 10^{38}$  ergs  $s^{-1}$ . The slope of the low-luminosity power law is  $\beta = 1.8 \pm 0.2$ , while that of the high-luminosity power law is  $\beta = 2.8 \pm 0.6$ . Note that the cumulative XLF slope below the break is similar to that obtained from the single power law model ( $\alpha \sim 1.1$ ), because  $\beta < \alpha + 1$  below the break (see Fig. 7 and § 5.2). The effect of this break is not a flattening of the low-luminosity XLF (compared to a single power law fit),

but a steepening of the XLF at higher luminosities: note that the high-luminosity slope is more uncertain, given the small number of very bright sources. This point is particularly important for the determination of the contribution from LMXBs to the integrated X-ray luminosity of the galaxies and will be discussed in §§ 4 and 5.

The break suggested by the fit of the combined XLF occurs at a higher luminosity (by a factor of  $\sim 2.5$ ) than  $L_{X,\text{Edd}} = 2 \times 10^{38}$  ergs  $s^{-1}$  (with a  $\sim 3 \sigma$  significance; see § 5.1). We exclude that the break luminosity could be the result of the wrong spectral assumptions producing apparently larger X-ray luminosities for these bright sources (see Finoguenov & Jones 2002), if they have a softer X-ray spectrum than assumed in the count rate to flux conversion. The spectral properties for sources with different  $L_X$  values are remarkably similar in NGC 1316 (KF03) and also in a large sample of early-type galaxies (Irwin et al. 2003); all these spectra tend to be rather hard.

We note that cosmic background X-ray sources, which contribute to  $\sim 10\%$  of the detected sources (Table 1, col. [17]) in our LMXB flux range (and within the  $D_{25}$  ellipse), exhibit a similar break in the  $\log N - \log S$  relation (e.g., Kim et al. 2004b; Hasinger et al. 1998). At the distance of the Virgo Cluster (17 Mpc), the break luminosity corresponds to  $\sim 5 \times 10^{38}$  ergs  $s^{-1}$ , similar to the location of the XLF break. To assess quantitatively the effect of the cosmic background X-ray sources, we added an extra broken power law component, based on the ChAMP  $\log N - \log S$  by Kim et al. (2004b), to the above fitting. The results are statistically consistent within the errors. Irwin et al. (2003) have recently suggested that very bright sources ( $L_X > 2 \times 10^{39}$  ergs  $s^{-1}$ ) found in early-type galaxies may be background AGNs. We have repeated our fitting with only sources of  $L_X < 2 \times 10^{39}$  ergs  $s^{-1}$  and again reached consistent results within the errors.

#### 4. TOTAL INTEGRATED X-RAY LUMINOSITY OF THE LOW-MASS X-RAY BINARY POPULATION

Using the individual XLFs, we can estimate the integrated X-ray luminosity of both detected and undetected sources in our sample of galaxies. Given the old stellar populations of these systems, pointlike X-ray sources are likely to be entirely

TABLE 3  
TOTAL X-RAY LUMINOSITY OF LOW-MASS X-RAY BINARIES

Name (1)	$L_X(1)$ (2)	Correction (3)	$L_X(2)$ (4)	$L_B$ (5)	$L_K$ (6)	$L_X(2)/L_B$ (7)	$L_X(2)/L_K$ (8)
I1459 .....	2.548	0.67	3.803	6.037	30.563	0.630	0.124
N0720.....	2.354	0.68	3.462	4.269	18.583	0.811	0.186
N1316.....	3.510	0.71	4.944	10.610	45.135	0.466	0.110
N1399.....	6.458	0.70	9.226	4.071	22.579	2.266	0.409
N1407.....	6.828	0.79	8.643	6.742	32.719	1.282	0.264
N3379.....	0.426	0.68	0.626	1.580	7.413	0.396	0.084
N4365.....	2.095	0.69	3.036	2.837	11.828	1.070	0.257
N4374.....	2.021	0.67	3.016	4.415	17.951	0.683	0.168
N4382.....	1.116	0.74	1.508	4.497	19.449	0.335	0.078
N4472.....	6.064	0.74	8.195	8.258	38.949	0.992	0.210
N4621.....	0.917	0.68	1.349	2.735	11.130	0.493	0.121
N4636.....	2.429	0.79	3.075	2.998	13.858	1.026	0.222
N4649.....	6.087	0.76	8.009	5.874	29.033	1.363	0.276
N4697.....	1.445	0.80	1.806	2.081	7.755	0.868	0.233

NOTES.—Col. (1): Galaxy name. Col. (2): X-ray luminosity (in  $10^{40}$  ergs  $s^{-1}$ ) of total discrete sources with  $L_X(\min) = 10^{37}$  ergs  $s^{-1}$  and  $L_X(\max) = 2 \times 10^{39}$  ergs  $s^{-1}$ . Col. (3): The correction factor is to take into account sources excluded because they are outside S3 and within  $20''$  of the center. Col. (4): Same as  $L_X(1)$  after adding sources outside S3 and in the central  $20''$ . Col. (5): Optical luminosity in  $B$  (in units of  $10^{10} L_\odot$ , with  $M_{B\odot} = 5.47$  mag). Col. (6): Near-IR luminosity in  $K$  (in units of  $10^{10} L_\odot$ , with  $M_{K\odot} = 3.33$  mag). Col. (7): X-ray to optical luminosity ratio in units of  $10^{30}$  ergs  $s^{-1}/L_{B\odot}$ . Col. (8): X-ray to near-IR luminosity ratio in units of  $10^{30}$  ergs  $s^{-1}/L_{K\odot}$ .

representative of LMXBs. Our results are summarized in Table 3. Because the XLF is steep ( $\beta \sim 2.1$ ), the total X-ray luminosity of LMXBs depends on the undetected lower  $L_X$  break of the XLF, which in our sample is below a few  $\times 10^{37}$  ergs  $s^{-1}$ . Following LMXBs detected in the Milky Way (Grimm et al. 2002) and in the bulge of M31 (Kong et al. 2002), we assume the lower limit to the XLF at  $10^{37}$  ergs  $s^{-1}$  and list the result in column (2) of Table 3. If we conservatively take a larger limit of  $4 \times 10^{37}$  ergs  $s^{-1}$ , which is the observational threshold of our sample,  $L_X$  decreases by 20%–25%. In column (3) we list a correction factor that takes into account the omission of sources from the XLFs, either because they did not fall in the S3 chips or because of the exclusion of the central  $20''$  of the galaxies from the XLF (see § 3). We assume that LMXBs are spatially distributed following the optical light ( $r^{1/4}$  law). The corrected total LMXB luminosities are listed in column (4). These luminosities range from a few  $\times 10^{39}$  to several  $\times 10^{40}$  ergs  $s^{-1}$ .

Table 3 lists the ratio  $L_X(\text{LMXB})/L_B$  in units of  $10^{40}$  ergs  $s^{-1}/10^{10} L_{B\odot}$ , where  $L_B$  represents the integrated stellar luminosity in the optical band.  $L_B$  was derived from  $B_T^0$ , the total face-on magnitude corrected for Galactic extinction (col. [8] of Table 1, taken from RC3), adopting  $M_{B\odot} = 5.47$  mag. The X-ray to optical ( $B$ ) luminosity ratios range from 0.3 to 1.7 (with the lowest in NGC 4382 and the highest in NGC 1399). The mean and standard deviation are

$$L_X(\text{LMXB})/L_B = (0.9 \pm 0.5) \times 10^{30} \text{ ergs } s^{-1}/L_{B\odot},$$

with  $L_X(\min) = 10^{37}$  ergs  $s^{-1}$ .

Our estimates are consistent with the previous measurements by Kim et al. (1992) and O’Sullivan et al. (2001), after correcting for the different energy bands used. However, the large scatter is statistically significant if the XLFs of individual E and S0 galaxies do not differ significantly below the detection threshold.

Also in Table 3 we list the ratio  $L_X(\text{LMXB})/L_K$ . We have introduced the  $K$ -band luminosity ( $L_K$ ) as an additional mea-

sure of the integrated stellar emission because the near-IR luminosity may be more appropriate for the old stellar population of early-type galaxies and also is less affected by extinction than the  $B$ -band luminosity.  $L_K$  was derived from  $K_{20}$  measured within the 20 mag arcsec $^{-2}$  isophote (col. [10] of Table 1, taken from 2MASS; Jarrett et al. 2003) and using  $M_{K\odot} = 3.33$  mag. With  $L_K$ , we obtain

$$L_X(\text{LMXB})/L_K = (0.20 \pm 0.08) \times 10^{30} \text{ ergs } s^{-1}/L_{K\odot},$$

with  $L_X(\min) = 10^{37}$  ergs  $s^{-1}$ .

Figure 6 shows the scatter diagram between  $L_X(\text{LMXB})$  against  $L_K$  for our 14 galaxies. Two extreme galaxies, NGC 1399 [with the highest  $L_X(\text{LMXB})/L_K$ ] and NGC 3379 (with the lowest  $L_K$ ), are marked by a large circle and a large square, respectively. This figure shows that there is considerable spread in X-ray to near-IR ratios. This scatter exceeds that expected from the uncertainties in the measurement of  $L_X(\text{LMXB})$ . The scatter of  $L_X(\text{LMXB})/L_K$  (Fig. 6) is  $\pm 0\%$  at  $1 \sigma$  rms. If we use  $L_B$ , the scatter is slightly larger,  $\pm 60\%$  at  $1 \sigma$  rms, in a good agreement with a factor of 4 scatter (in a full width) reported by White et al. (2002). We further discuss the  $L_X(\text{LMXB})/L_K$  scatter in § 5.3.

Nevertheless, significant correlations exist between  $L_X(\text{LMXB})$  and both  $L_B$  and  $L_K$  (see Fig. 6). The Spearman rank correlation coefficients are 0.71 and 0.82, corresponding to chance probabilities of 1% and 0.3% for the  $B$  and  $K$  correlations, respectively, confirming the tighter correlation with  $L_K$ . Also plotted in Figure 6 is the bulge of the Milky Way (*star*) and M31 (*asterisk*). For the Milky Way, the optical luminosity of the bulge was taken from Cox (2000) and the X-ray luminosity of LMXBs from Grimm et al. (2002), while for M31, the optical luminosity is from Kent (1989) and the X-ray luminosity from Trinchieri & Fabbiano (1991).  $L_X$  was rescaled for the energy range of 0.3–8 keV. The near-IR luminosity ( $L_K$ ) was estimated using the average  $B - K$  color (or  $L_K/L_B = 4.5$ ) in our sample of early-type galaxies. Although these quantities are somewhat uncertain (e.g., Widrow

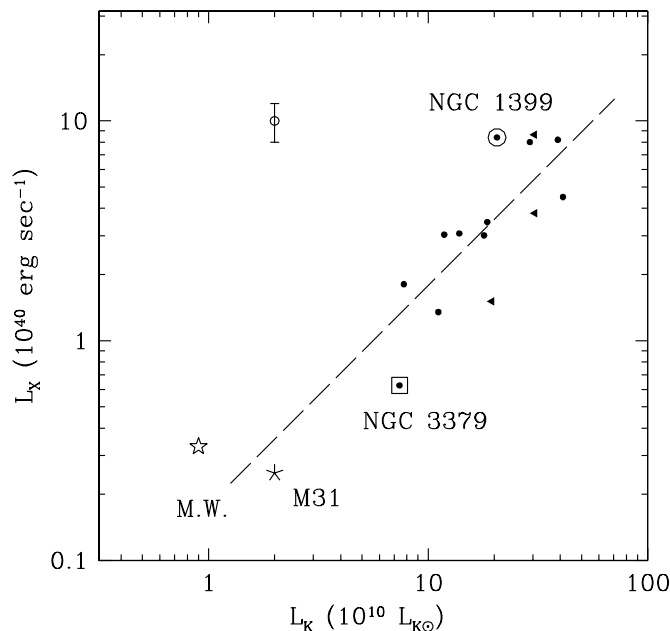


FIG. 6.—X-ray luminosity of LMXBs,  $L_X$ (LMXB), plotted against the near-infrared luminosity  $L_K$ . The dashed line indicates the linear relation (slope = 1.0). Two extreme galaxies, NGC 1399 [with the highest  $L_X$ (LMXB)/ $L_K$ ] and NGC 3379 (with the lowest  $L_K$ ), are marked by a large circle and a large square, respectively. Three galaxies with no GC data are marked with triangles (to be consistent with Fig. 8). A typical error bar is shown in the top left corner. Also plotted are the bulges of the Milky Way (*star*) and M31 (*asterisk*) (see text).

et al. 2003 suggested a lower [by a factor of 2] M31 bulge mass than measured by Kent 1989), the bulges of the Milky Way and M31 follow the general trend of early-type galaxies and roughly indicate the upper and lower bounds of the  $L_X/L_K$  scatter (see § 5.2 for more comparisons).

## 5. DISCUSSION

### 5.1. The XLF of Early-Type Galaxies

The study of the X-ray source populations of early-type galaxies detected with *Chandra* has generated a considerable amount of excitement and some controversy. Excitement because we finally have irrefutable proof of the existence of these sources (e.g., Sarazin et al. 2000), which had been predicted on the basis of indirect evidence since the first observations of early-type galaxies with the *Einstein Observatory* (Trinchieri & Fabbiano 1985; see Fabbiano 1989). Controversy because of the derivation and interpretation of the XLFs of these X-ray source populations: the early suggestion (e.g., Sarazin et al. 2000; Blanton et al. 2001) of a universal break in the XLFs at the Eddington luminosity of neutron stars ( $L_{X,\text{Edd}} \sim 2 \times 10^{38}$  ergs  $\text{s}^{-1}$ ) was later related to the lack of careful incompleteness corrections (KF03, for NGC 1316; see also Sivakoff et al. 2003 for NGC 4365 and NGC 4382). The lack of a signature at the Eddington luminosity is intriguing because this effect is expected if the emission of X-ray binaries is Eddington-limited, as demonstrated by synthetic XLFs based on binary evolution models (Kalogera et al. 2003).

The purpose of the work reported in this paper is to address the issue of the shape of the XLF by performing a rigorous analysis of a representative sample of E and S0 galaxies, leading to a set of uniformly derived completeness-corrected XLFs. As reported in § 3, to a first approximation all these

XLFs are well fitted with single power law models, with best-fit (differential) slopes ranging from 1.7 to 2.2. Comparing these results with a set of synthetic XLFs, we conclude that this apparent variety may be the result of small-number statistics (typically 100 sources or less are involved in each XLF). We do not find any strong statistical evidence of breaks at  $L_{X,\text{Edd}}$  in these XLFs, and we therefore conclude that incompleteness played a role in the early reports of this feature (e.g., Sarazin et al. 2000; Blanton et al. 2001).

Nonetheless, we find evidence of a break when we create a composite XLF for the entire sample, under the working assumption that there is a “universal” XLF shape of the X-ray source population of old stellar systems. This composite XLF may suggest a departure from a simple power-law distribution, consistent with having a break at a luminosity of  $5 \times 10^{38}$  ergs  $\text{s}^{-1}$ . If this break is real, its luminosity may be inconsistent with the  $L_{X,\text{Edd}}$  of  $1.4 M_\odot$  neutron stars (at  $3 \sigma$  confidence) but would be consistent with the  $3 M_\odot$  upper limit on the neutron star mass suggested by Kalogera & Baym (1996). This break could also correspond to the Eddington luminosity of a  $\sim 3.5 M_\odot$  accreting black hole. Another possibility for the super-Eddington luminosity is He-enriched accretion, which could effectively double  $L_{X,\text{Edd}}$  because of the smaller cross section per unit mass (see, e.g., Shakura & Sunyaev 1973; Grimm et al. 2003). Podsiadlowski et al. (2002) suggested that a large fraction of LMXBs might have started as intermediate-mass (neutron star) X-ray binaries with an initial mass of companion star  $\sim$  a few  $M_\odot$ . Because these systems would be in a later evolutionary stage (than a typical LMXB with  $< 1 M_\odot$ ), they could be hydrogen-deficient and helium-enriched, and hence the Eddington accretion rate may be considerably enhanced. However, these systems are relatively short-lived (Podsiadlowski et al. 2002), and while they may be present in young E/S0 galaxies such as Fornax A and Cen A, they are not likely to be found in the old elliptical galaxies of our sample (Trager et al. 2000).

If the change in XLF slope is real and does not mask a step in the XLF that is not detectable because of the relative low number of high-luminosity sources, our result implies that there are two different source populations, neutron star and black hole binaries, with different XLFs (see Sarazin 2000). A step in the XLF would be more indicative of a beaming effect that may enhance the luminosity of some high accretion rate binaries (King 2002). In the latter case, we may expect that the fraction of sources with “enhanced” apparent luminosity would have the same luminosity function slope as their parent population, the unbeamed LMXBs. If the above consideration continues to hold for future observations, the high-luminosity portion of the XLF could reflect the mass function of black holes in elliptical galaxies. We note that this high-luminosity population does not resemble that of the ultra-luminous sources detected in star-forming galaxies, where no break in the XLF is present and where the power-law slope is much flatter than in the older stellar system we are studying here (see Fabbiano & White 2003 and references therein). Analysis of a larger sample is needed to firmly establish the behavior of the high-luminosity portion of the XLF of LMXBs.

### 5.2. Comparison with the LMXB XLFs of M31 and the Galaxy

Figure 7 compares our composite cumulative XLF with the XLFs of the LMXBs found in the bulge of M31 (Kong et al. 2002), those matched with the GCs of M31 (Kong et al. 2003),

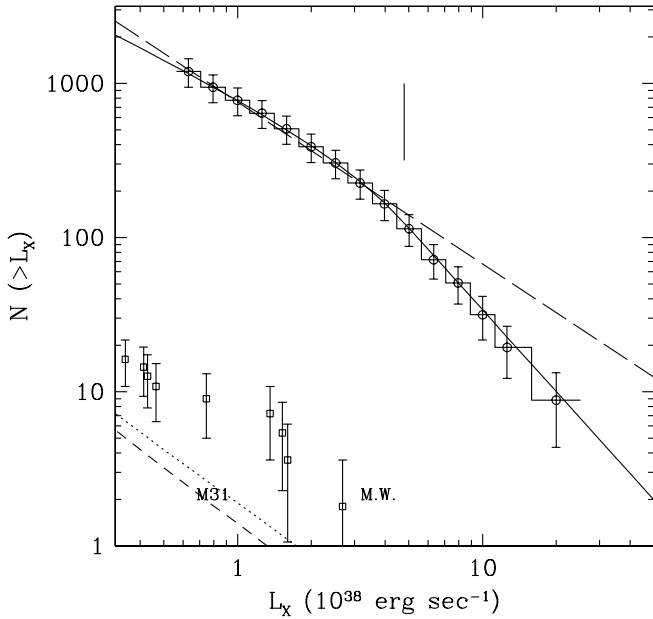


FIG. 7.—Cumulative XLF of the 14 E and SO galaxies. The long-dashed and solid lines are the best-fit single power law and broken power law. The vertical bar at the top indicates the break  $L_X$  in the broken power law fit. Also plotted in the bottom left corner are XLFs determined from LMXBs in the Milky Way (squares with error bars) and M31 (dotted line, bulge sources; dashed line, GC sources).

and the LMXBs in the Milky Way (Grimm et al. 2002). The similarity of the shapes of these three luminosity functions, in the luminosity range covered by our XLF, is remarkable and suggests that we are indeed looking at similar X-ray binary populations. The cumulative power-law slopes determined by Kong et al. (2002, 2003) for the bulge of M31 and for the GCs of M31 ( $\beta = 2.15$  at  $L_X > 0.8 \times 10^{37}$  ergs  $s^{-1}$  and  $\beta = 2.2$  at  $L_X > 2 \times 10^{37}$  ergs  $s^{-1}$ ) compare well with our cumulative XLF,  $\beta = 2.1 \pm 0.1$  for a single power law or  $\beta = 1.8 \pm 0.2$  at luminosities below the break ( $5 \times 10^{38}$  ergs  $s^{-1}$ ) for a broken power law (note that even in the broken power law fit, the cumulative XLF slope below the break is close to  $\alpha = 1.1$ ). The LMXBs in the Milky Way (Grimm et al. 2002) show the same trend. A significant difference in both the M31 and Milky Way LMXB XLFs is the absence of the luminous sources ( $L_X > 2 \times 10^{38}$  ergs  $s^{-1}$ ) that we detect in E and SO galaxies. However, this could be just a result of population statistics, given the smaller population sizes of the bulge of M31 and the Milky Way when compared with our sample E and SO galaxies. For example, for a given  $L_B$  of the Milky Way bulge, we expect only a few LMXBs with  $L_X > 10^{38}$  ergs  $s^{-1}$ , consistent with observations (e.g., Grimm et al. 2002).

In both the M31 and the Milky Way LMXB XLFs, there is a low-luminosity break near  $L_X \sim 10^{37}$  ergs  $s^{-1}$ , and the slope flattens considerably at lower luminosities. This luminosity range is well below the sensitivity of the *Chandra* observations used in this study. Only in NGC 3379, the nearest galaxy in our sample, can we detect sources with luminosities as low as  $L_X = 2 \times 10^{37}$  ergs  $s^{-1}$  (see the bottom XLF in Figs. 1 and 2), and in this case the low-luminosity break is not seen. Given the similarity between all these XLFs, it is reasonable to assume that there may be a low-luminosity break in the XLFs of E and SO at a similar luminosity, as seen in M31 and the Milky Way. Based on the LMXBs found in the Milky Way

(Grimm et al. 2002), the integrated X-ray luminosity of LMXBs with  $L_X < 10^{37}$  ergs  $s^{-1}$  is only  $\sim 8\%$  of the total LMXB emission.

### 5.3. The $L_X(\text{LMXB})/L_{\text{opt}}$ Relation and the Evolution of LMXBs

With the detection of X-ray source populations in early-type galaxies, there has been renewed interest in probing the formation of these systems, and in particular in exploring a possible evolutionary link to GCs, originally suggested by Grindlay (1984) as the main formation mechanism for Galactic LMXBs. A significant fraction of the sources detected with *Chandra* in early-type galaxies are associated with GCs (e.g., Angelini et al. 2001; Kundu et al. 2002; see compilation in Fabbiano & White 2003). This association has led to the suggestion that GCs may be the birthplace of the entire LMXB population, from where they may be expelled if they receive strong enough formation “kicks,” or left behind upon tidal disruption of the parent cluster (see Sarazin et al. 2000; White et al. 2002).

Following White et al. (2002), who suggested a correlation of the  $L_X(\text{LMXB})/L_{\text{opt}}$  ratio with the GC specific frequency, we explored the behavior of the  $L_X(\text{LMXB})/L_{\text{opt}}$  ratio of our sample to see if we could find any trends. Our advantage is that our study of the XLF should result in the most rigorous determination of the integrated LMXB luminosities. Furthermore, because we find that the shape of LMXB XLFs is uniform, the correlation, if confirmed, directly indicates that the number of LMXBs is proportional to the number of GCs in individual E/SO galaxies. This would in turn provide strong evidence that LMXBs are mainly, if not entirely, formed in GCs.

While the global stellar content (measured by the optical or near-IR light) is correlated with the integrated luminosity of LMXBs (Fig. 6), the scatter seems to require a secondary parameter. Using the  $L_X(\text{LMXB})/L_K$  ratio, which has the least amount of scatter (see § 4), we explore dependencies of the scatter from a second parameter in Figure 8, where we plot this ratio versus  $L_K$  and versus the GC specific frequency  $S_{\text{GC}}$  defined by the number of GCs per unit galaxy luminosity:

$$S_{\text{GC}} = N_{\text{GC}} \times 10^{0.4(M_v + 15)}.$$

$S_{\text{GC}}$  was estimated from the GC data listed in Table 1. NGC 1407, NGC 4382, and IC 1459 do not have  $S_{\text{GC}}$  data and are marked by triangles at the left side of Figure 8.

For comparison, we plot the Milky Way (and M31) by rescaling  $S_{\text{GC}} = 0.5$  (and 0.7) of the whole Galaxy (Harris 1991) for the bulge luminosity (Cox 2000; Kent 1989). However, we note that this is subject to a large uncertainty because this quantity may not be simply scalable (e.g., by local/global variations).

Figure 8a shows that there is no dependency of  $L_X(\text{LMXB})/L_K$  on the integrated stellar luminosity ( $L_K$ ). Instead (Fig. 8b), there is a suggestion of a correlation with  $S_{\text{GC}}$ , which would follow the suggestion of White et al. (2002). The Spearman rank correlation test gives a chance probability of 2%. However, if we exclude NGC 1399, which is the galaxy with the largest  $S_{\text{GC}}$  (marked by the large circle in the top right corner of Fig. 8b), the chance probability increases to 5%. We note that another known elliptical galaxy with a very high  $S_{\text{GC}}$ , NGC 4486, which hosts twice as many GCs as NGC 1399 (Kissler-Patig 1997), does not have as many LMXBs as in

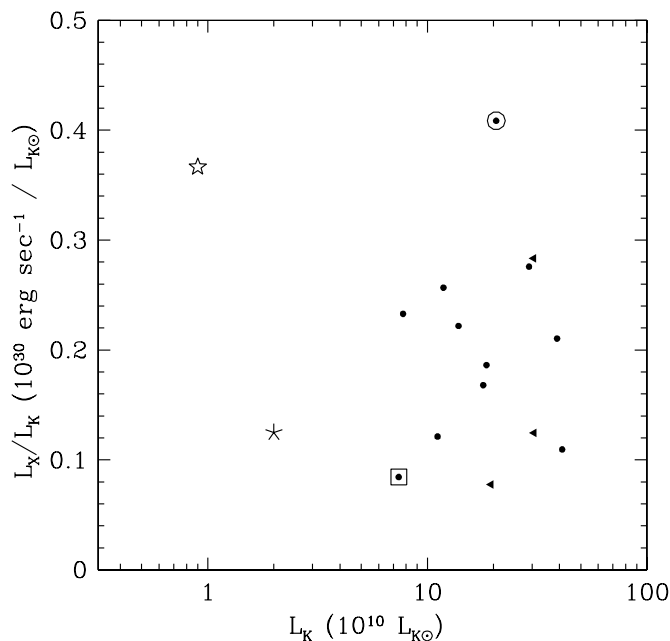


FIG. 8a

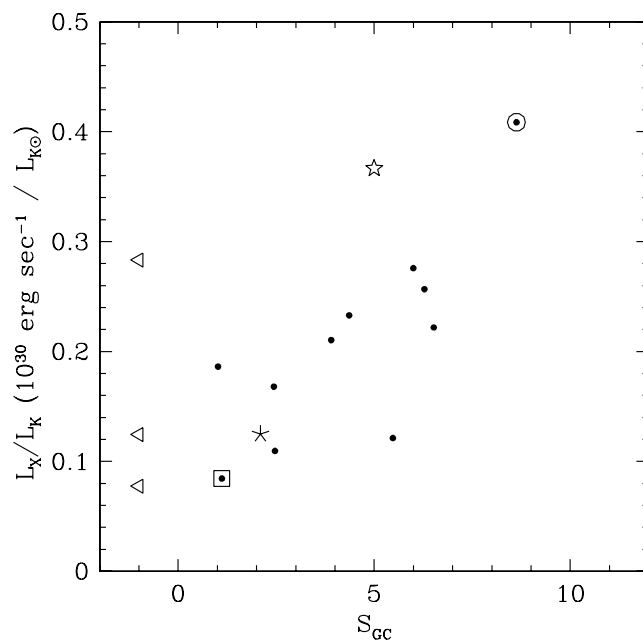


FIG. 8b

FIG. 8.— $L_X(\text{LMXB})/L_K$  plotted against (a)  $L_K$  and (b) the GC specific frequency ( $S_{GC}$ ). Two extreme galaxies, NGC 1399 [with the highest  $L_X(\text{LMXB})/L_K$ ] and NGC 3379 (with the lowest  $L_K$ ), are marked by a large circle and a large square, respectively. Three galaxies with no  $S_{GC}$  data are marked with triangles. Also plotted are the bulges of the Milky Way (*star*) and M31 (*asterisk*) (see text).

NGC 1399 (E. Kim et al. 2004, in preparation), indicating that NGC 1399 may not follow the general trend of early-type galaxies. We also note that the measured  $S_{GC}$  values vary considerably; for example, the  $S_{GC}$  of NGC 4374 differs by a factor of 2.4 between Kissler-Patig (1997) and Gomez & Richtler (2004). In conclusion, although there is a weak suggestion of a connection between  $S_{GC}$  and  $L_X(\text{LMXB})/L_K$ , this is by no means an established result. The LMXB-GC connection is still an open issue that needs to be confirmed with a larger sample of galaxies with well-determined  $S_{GC}$  values.

Based on the GC-LMXB connection, one might expect that the radial distribution of LMXBs is similar to that of GCs and hence flatter than that of the optical halo light. However, using ground and *Hubble Space Telescope* observations of six giant elliptical galaxies, E. Kim et al. (2004, in preparation) find that LMXBs follow the optical halo light more closely than more extended GCs, suggesting a rather complex connection, if any, depending on various factors operating in LMXB formation in GCs and its subsequent evolution. The close agreement between the radial distributions of the optical light and LMXBs is also seen in NGC 1316 (KF03). This justifies our usage of the  $r^{-1/4}$  law for the LMXB distribution (§§ 3.1 and 4). As already suggested by Kundu et al. (2002) and Sarazin et al. (2003), E. Kim et al. (2004, in preparation) confirm a significantly higher probability (by a factor of 4) of finding LMXBs in red (metal-rich) GCs than in blue (metal-poor) GCs, indicating that metal abundance may play a key role in forming LMXBs (e.g., by a flatter initial mass function or by irradiation-induced stellar winds, as suggested by Maccarone et al. 2004). The observed radial behavior of LMXBs may be partly understood because red GCs are often more centrally concentrated than blue GCs (Lee et al. 1998; see also E. Kim et al. 2004, in preparation). However, there may be other factors, such as variable capture rates as a

function of cluster density, which could make the LMXB distribution look steeper.

## 6. CONCLUSIONS

We have derived bias-corrected XLFs in the range  $L_X = 2 \times 10^{37}$  to  $2 \times 10^{39}$  ergs  $s^{-1}$  for a uniformly selected sample of 14 E and S0 galaxies observed with *Chandra* ACIS-S3, following the approach of KF03. The entire sample yields 985 pointlike X-ray sources, with 30–140 sources detected per galaxy. Our analysis shows the following:

1. After correcting for incompleteness, the individual XLFs are statistically consistent with a single power law of a (differential) slope  $\beta = 1.8$ – $2.2$ . A break at or near  $L_{X,\text{Edd}}$ , as reported in the literature for some of these galaxies (see review in Fabbiano & White 2003), is not required in any case. We also demonstrate, by comparison with simulated data generated from the same parent power-law XLF, that the apparent differences in the shape of each individual XLF are consistent within statistics.

2. Given that all the XLFs have statistically consistent shapes, we have combined the entire data set to generate a representative XLF of X-ray sources in elliptical galaxies, with increased sensitivity. Although the combined XLF is marginally consistent with a single power law, a broken power law gives an improved fit. The best-fit (differential) slope is  $\beta = 1.8 \pm 0.2$  in the low-luminosity range  $L_X = \text{a few} \times 10^{37}$  to  $5 \times 10^{38}$  ergs  $s^{-1}$ . At higher luminosities, the slope is steeper,  $\beta = 2.8 \pm 0.6$ . The break luminosity is  $(5 \pm 1.6) \times 10^{38}$  ergs  $s^{-1}$ . We note that the low-luminosity slope (in a cumulative form) is consistent with that obtained from the single power law model ( $\alpha = 1.1 \pm 0.1$ ;  $\beta < \alpha + 1$  below the break). We find that the break luminosity is not significantly altered by either spectral or distance uncertainties in our sample or by contamination by background AGNs.

3. If the XLF is indeed broken, the break luminosity may be higher than  $L_{X,\text{Edd}}$  of a  $1.4 M_{\odot}$  neutron star (at  $\sim 3 \sigma$  confidence) but consistent with the Eddington luminosity of the largest possible neutron star mass proposed ( $3 M_{\odot}$ ; Kalogera & Baym 1996). This break luminosity is in the range of  $L_{X,\text{Edd}}$  values of stellar mass black holes. Alternatively, a He-enriched LMXB could also be consistent with a larger  $L_{X,\text{Edd}}$  value. If the change in slope is real and does not mask a step in the XLF that is not detectable because of the relatively low number of high-luminosity sources, our result implies a different population of high-luminosity sources, instead of a beaming effect. This high-luminosity portion of the XLF could reflect the mass function of black holes in these galaxies. We note that this high-luminosity population does not resemble that of the ultra-luminous sources detected in star-forming galaxies, where no break in the XLF is present. Also, the power-law slope is much flatter in star-forming galaxies than in the older stellar system we are studying here (see Fabbiano & White 2003 and references therein).

4. Within statistics, our low-luminosity composite XLF is fully consistent with the XLFs of LMXBs of the Milky Way (Grimm et al. 2002) and of both the bulge and GCs of M31 (Kong et al. 2002, 2003). The proximity of the Milky Way and M31 sources allows a measurement of their XLFs down to significantly lower luminosities, demonstrating that the single power law (with  $\beta \simeq 2.2$ ) continues down to  $L_X \simeq 10^{37}$  ergs  $\text{s}^{-1}$ .

5. In contrast to the uniform XLF slope, the normalization of the XLFs varies widely from one galaxy to another, reflecting

the varying content of LMXBs. The total X-ray luminosity of LMXBs is correlated with both optical and (better) near-IR luminosities, but in both cases the scatter exceeds that expected from measurement errors. The regression lines are

$$L_X(\text{LMXB})/L_B = (0.9 \pm 0.5) \times 10^{30} \text{ ergs s}^{-1}/L_{B\odot},$$

$$L_X(\text{LMXB})/L_K = (0.2 \pm 0.08) \times 10^{30} \text{ ergs s}^{-1}/L_{K\odot}.$$

6. Following White et al. (2002), we find that the scatter in  $L_X(\text{LMXB})/L_K$  is marginally correlated with the specific frequency of GCs ( $S_{\text{GC}}$ ), suggesting an important role of GCs in LMXB evolution. This conclusion, however, needs to be confirmed with a larger sample of galaxies with accurately measured  $S_{\text{GC}}$  values.

*Note added in manuscript.*—After submitting this paper, we became aware that Gilfanov (2004) has reached conclusions consistent with ours (on the XLF shape and the break luminosity) with different samples and by independent approaches.

This work was partly supported by NASA grant NAS8-39073 (CXC). We thank H.-J. Grimm for providing the Milky Way data, V. Kashyap for discussing statistics issues, and M. Elvis for carefully reading the draft.

#### REFERENCES

- Allen, S. W., Di Matteo, T., & Fabian, A. C. 2000, MNRAS, 311, 493  
 Angelini, L., Loewenstein, M., & Mushotzky, R. F. 2001, ApJ, 557, L35  
 Belczynski, K., Kalogera, V., Zezas, A., & Fabbiano, G. 2004, ApJ, 601, L147  
 Blanton, E. L., Sarazin, C. L., & Irwin, J. A. 2001, ApJ, 552, 106  
 Cox, A. N., ed. 2000, Allen's Astrophysical Quantities (4th ed.; New York: AIP)  
 Crawford, D. F., Jauncey, D. L., & Muldoch, H. S. 1970, ApJ, 162, 405  
 de Vaucouleurs, G. 1948, Ann. d'Astrophys., 11, 247  
 de Vaucouleurs, G., de Vaucouleurs, H., Corwin, H. G., Jr., Buta, R. J., Paturel, G., & Fouqué, P. 1991, Third Reference Catalogue of Bright Galaxies (New York: Springer) (RC3)  
 Eskridge, P. B., Fabbiano, G., & Kim, D.-W. 1995, ApJS, 97, 141  
 Fabbiano, G. 1989, ARA&A, 27, 87  
 Fabbiano, G., & White, N. E. 2003, preprint (astro-ph/0307077)  
 Fabbiano, G., et al. 2003, ApJ, 588, 175  
 Fasano, G., Pisani, A., Vio, R., & Girardi, M. 1993, ApJ, 416, 546  
 Finoguenov, A., & Jones, C. 2002, ApJ, 574, 754  
 Freeman, P., & Kashyap, V. 2002, ApJS, 138, 185  
 Gilfanov, M. 2004, MNRAS, 349, 146  
 Gilfanov, M., Grimm, H.-J., & Sunyaev, R. 2003, preprint (astro-ph/0309725)  
 Gomez, M., & Richtler, T. 2004, A&A, 415, 499  
 Goudfrooij, P., Alonso, M. V., Maraston, C., & Minniti, D. 2001, MNRAS, 328, 237  
 Grimm, H.-J., Gilfanov, M., & Sunyaev, R. 2002, A&A, 391, 923  
 Grindlay, J. E. 1984, Adv. Space Res., 3, 19  
 Harris, W. E. 1991, ARA&A, 29, 543  
 Hasinger, G., Burg, R., Giacconi, R., Schmidt, M., Trümper, J., & Zamorani, G. 1998, A&A, 329, 482  
 Irwin, J. A., Athey, A. E., & Bregman, J. N. 2003, ApJ, 587, 356  
 Jarrett, T. H., Chester, T., & Cutri, R. 2003, AJ, 125, 525  
 Jeltema, T. E., Canizares, C. R., Buote, D. A., & Garmire, G. P. 2003, ApJ, 585, 756  
 Jones, C., et al. 2002, ApJ, 567, L115  
 Kalogera, V., & Baym, G. 1996, ApJ, 470, L61  
 Kalogera, V., Belczynski, C., Zezas, A., & Fabbiano, G. 2003, in Globular Clusters: Formation, Evolution, and the Role of Compact Objects, ed. L. Bildsten et al. (Santa Barbara: KITP), [http://online.kitp.ucsb.edu/online/clusters\\_c03](http://online.kitp.ucsb.edu/online/clusters_c03)  
 Kent, S. 1989, AJ, 97, 1614  
 Kim, D.-W., & Fabbiano, G. 2003, ApJ, 586, 826 (KF03)  
 Kim, D.-W., Fabbiano, G., & Trinchieri, G. 1992, ApJ, 393, 134  
 Kim, D.-W., et al. 2004a, ApJS, 150, 19  
 ———. 2004b, ApJ, 600, 59  
 King, A. R. 2002, MNRAS, 335, L13  
 Kissler-Patig, M. 1997, A&A, 319, 83  
 Kong, A. K. H., Di Stefano, R., Garcia, M. R., & Greiner, J. 2003, ApJ, 585, 298  
 Kong, A. K. H., Garcia, M. R., Primini, F. A., Murray, S. S., Di Stefano, R., & McClintock, J. E. 2002, ApJ, 577, 738  
 Kundu, A., Maccarone, T. J., & Zepf, S. E. 2002, ApJ, 574, L5  
 Lee, M. G., Kim, E., & Geisler, D. 1998, AJ, 115, 947  
 Maccarone, T. J., Kundu, A., & Zepf, S. E. 2004, ApJ, 606, 430  
 Matsushita, K., et al. 1994, ApJ, 436, L41  
 O'Sullivan, E., Forbes, D. A., & Ponman, T. J. 2001, MNRAS, 328, 461  
 Podsiadlowski, Ph., Rappaport, S., & Pfahl, E. D. 2002, ApJ, 565, 1107  
 Randall, S. W., Sarazin, C. L., & Irwin, J. A. 2004, ApJ, 600, 729  
 Rhode, K. L., & Zepf, S. E. 2004, AJ, 127, 302  
 Sarazin, C. L., Irwin, J. A., & Bregman, J. N. 2000, ApJ, 544, L101  
 ———. 2001, ApJ, 556, 533  
 Sarazin, C. L., Kundu, A., Irwin, J. A., Sivakoff, G. R., Blanton, E. L., & Randall, S. W. 2003, ApJ, 595, 743  
 Shakura, N., & Sunyaev, R. 1973, A&A, 24, 337  
 Sivakoff, G. R., Sarazin, C. L., & Irwin, J. A. 2003, ApJ, 599, 218  
 Stark, A. A., et al. 1992, ApJS, 79, 77  
 Tonry, J. L., et al. 2001, ApJ, 546, 681  
 Trager, S. C., Faber, S. M., Worthey, G., & Gonzalez, J. J. 2000, AJ, 120, 165  
 Trinchieri, G., & Fabbiano, G. 1985, ApJ, 296, 447  
 ———. 1991, ApJ, 382, 82  
 Weisskopf, M. C., Tananbaum, H., Van Speybroeck, L. P., & O'Dell, S. L. 2000, Proc. SPIE, 4012, 2  
 White, R. E., III, Sarazin, C. L., & Kulkarni, S. R. 2002, ApJ, 571, L23  
 Widrow, L. M., Perrett, K. M., & Suyu, S. H. 2003, ApJ, 588, 311  
 Zezas, A., & Fabbiano, G. 2002, ApJ, 577, 726